# Synthesis and Characterization of Biotinylated Forms of Insulin-like Growth Factor-1: Topographical Evaluation of the IGF-1/IGFBP-2 and IGFBP-3 Interface † , ‡

**ARTICLE** *in* BIOCHEMISTRY · OCTOBER 2004

Impact Factor: 3.02 · DOI: 10.1021/bi049082k · Source: PubMed



**2 AUTHORS**, INCLUDING:

Steven A Rosenzweig
Medical University of South Carolina
**67** PUBLICATIONS **1,455** CITATIONS

SEE PROFILE

# Synthesis and Characterization of Biotinylated Forms of Insulin-like Growth Factor-1: Topographical Evaluation of the IGF-1/IGFBP-2 and IGFBP-3 Interface[†,‡]

Stephanie A. Robinson and Steven A. Rosenzweig*

*Department of Cell and Molecular Pharmacology and Experimental Therapeutics and Hollings Cancer Center, Medical University of South Carolina, 173 Ashley Avenue, Charleston, South Carolina 29425*

*Received May 6, 2004; Revised Manuscript Received July 8, 2004*

ABSTRACT: Activation of the insulin-like growth factor-1 (IGF)-1 receptor signaling pathways by IGF-1 and IGF-2 results in mitogenic and anabolic effects. The bioavailability of the IGFs is regulated by six soluble binding proteins, the insulin-like growth factor binding proteins (IGFBPs), which bind with ∼0.1 nM affinity to the IGFs and often serve as endogenous antagonists of IGF action. To identify key domains of IGF-1 involved in the interaction with IGFBP-2 and IGFBP-3, we employed IGF-1 selectively biotinylated on residues Gly 1, Lys 27, Lys 65, and Lys 68. All monobiotinylated species of IGF-1 exhibited high affinity (∼0.1−0.2 nM) for IGFBP-2 and IGFBP-3 in solid-phase-binding assays. However, different labeling intensities were observed in ligand blot analysis of IGFBP-2 and IGFBP-3. The $N^{\epsilon Lys65/68}$(biotin)-IGF-1 ($N^{\epsilon Lys65/68b}$-IGF-1) probe exhibited the highest signal intensity, while $N^{\alpha Gly1b}$-IGF-1 and $N^{\epsilon Lys27b}$-IGF-1 demonstrated significantly lower signals. When taken together, these results suggest that, once bound to IGFBP-2 or IGFBP-3, the biotin moieties of $N^{\alpha Gly1b}$-IGF-1 and $N^{\epsilon Lys27b}$-IGF-1 are inaccessible to NeutrAvidin-peroxidase, the secondary binding component. Ligand blots using IGF-1 derivatized with a long chain form of the *N*-hydroxysuccinimide biotin (NHS-biotin) to yield $N^{\alpha Gly1}$(LC-biotin)-IGF-1 and $N^{\epsilon Lys27}$(LC-biotin)-IGF-1 demonstrated increased signal intensity compared with their NHS-biotin counterparts. In BIAcore analysis, IGFBP-2 and IGFBP-3 bound only to the $N^{\epsilon Lys65/68b}$-IGF-1-coated flowcell of a biosensor chip, confirming the inaccessibility of Gly 1 and Lys 27 when IGF-1 is bound to IGFBP-2 and IGFBP-3. These data confirm the involvement of the IGFBP-binding domain on IGF-1 in binding to IGFBP-2 and IGFBP-3 and support involvement of the IGF-1R-binding domain in IGFBP binding.

The insulin-like growth factor (IGF)[1] system is a major contributor to cell survival. IGF-1 and IGF-2 are ∼7 kDa polypeptides exhibiting 70% sequence identity (*1*) and play important roles in fetal development; IGF-1 is primarily responsible for postnatal growth and tissue homeostasis into adulthood (*2*). The liver is the major source of circulating IGFs, although most tissues synthesize the IGFs locally (*3*). Therefore, the IGFs may act in an endocrine, paracrine, and/or autocrine fashion. The IGF-1 receptor (IGF-1R), a receptor tyrosine kinase, mediates the mitogenic effects of IGF-1 and IGF-2. Ligand affinities for the IGF-1R range from ∼1 nM (IGF-1) to 10 nM (IGF-2) to 1 $\mu$M (insulin) (*4*). The IGFs are regulated by a family of six IGF-binding proteins (IGFBPs), ranging in size from 22 to 31 kDa (*5*). The IGFBPs are characterized as natural antagonists of IGF action, on the basis of their exquisitely high affinity for the IGFs and their ability to inhibit IGF-mediated effects in vitro and in vivo (*6*−*11*). In addition, the IGFBPs prolong the serum half-life of the IGFs (*12*), deliver ligand to target tissues, and more recently have been shown to possess IGF-1/IGF-1R independent effects (*13*, *14*). Bioavailability of the IGFs is further regulated by proteases, such as prostate-specific antigen (PSA) (*15*) and the matrix metalloproteinases (*16*), which disrupt the interaction of the IGFBPs with the IGFs. The IGFBPs bind the IGFs with high affinity ($K_D$ = ∼0.1 nM) but demonstrate minimal affinity for insulin. However, Yamanaka et al. demonstrated that $^{125}$I-insulin or $^{125}$I-IGFs can be displaced from IGFBP-3 or the IGFBP-related protein (IGFBPrp), IGFBP-7/mac25, by either insulin or the IGFs, suggesting that these proteins bind at a site common to both the IGFs and insulin (*17*), such as their homologous receptor-binding domains. These data also indicate that the N terminus of IGFBP-3 may bind to the receptor-binding domains of IGF and insulin based on the observation that the IGFBPrps share homology with the N-terminal region of the IGFBPs (*18*). Furthermore, a

[†] This work was supported, in part, by a grant from the National Institutes of Health (CA-78887) and a Department of Defense grant to Hollings Cancer Center, (N6311601MD10004) to Steven A. Rosenzweig. Stephanie A. Robinson is supported by a dissertation research award from the Susan G. Komen Breast Cancer Foundation (DISS-0201947).

[‡] A portion of this work was presented at the 86th Annual Meeting of the Endocrine Society, June 2003, Philadelphia, Pennsylvania.

* To whom correspondence should be addressed: Department of Cell and Molecular Pharmacology and Experimental Therapeutics, Medical University of South Carolina, 173 Ashley Avenue, Charleston, SC 29425. Phone: 843-792-5841. Fax: 843-792-2475. E-mail: rosenzsa@musc.edu.

[1] Abbreviations: IGF, insulin-like growth factor; IGF-1R, insulin-like growth factor-1 receptor; IR, insulin receptor; IGFBP, insulin-like growth factor binding protein; IGFBPrp, insulin-like growth factor binding-protein-related protein; NMR, nuclear magnetic resonance; NHS-biotin, *N*-hydroxysuccinimide biotin; MALDI−TOF MS, matrix-assisted laser desorption ionization−time-of-flight mass spectrometry; RP-HPLC, reverse-phase-high-pressure liquid chromatography; CM, conditioned medium; ECL, enhanced chemiluminescence; QB-IGF-1, tetrabiotinylated IGF-1; SA, streptavidin.

10.1021/bi049082k CCC: $27.50 
Published on Web 08/18/2004

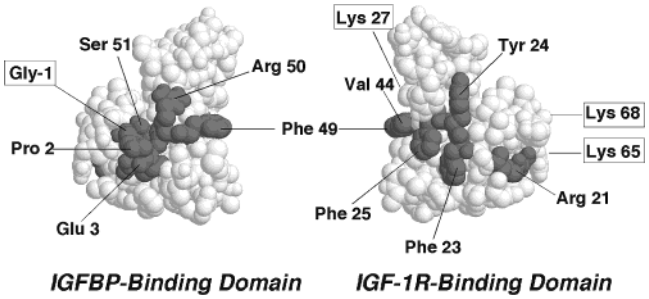


FIGURE 1: Binding domains on IGF-1. The designation of specific binding domains on IGF-1 is based on the minimized structure of IGF-1 obtained by NMR and structure−activity studies (*24*). The IGFBP-binding domain of IGF-1 is composed of residues Gly 1, Pro 2, Glu 3, Phe 49, Arg 50, and Ser 51 (left panel). The IGF-1R-binding domain, found on the opposite face of IGF-1, is made up of amino acids Val 44, Tyr 24, Arg 21, Phe 23, and Phe 25 (right panel). Gly 1, Lys 27, Lys 65, and Lys 68 are the sites of biotinylation. The image shown was obtained using Rasmol version 2.6 with coordinates from the Brookhaven National Laboratory Protein database (PDB 2gf1).

fragment of IGFBP-3 (1−87) demonstrated reduced but appreciable affinity for IGF-1 and increased affinity for insulin compared with full-length IGFBP-3 (*17*). Alterations in IGF system components, such as decreased IGFBP production (*19*), increased IGF-1R expression (*20*) and IGF-1 elevation in serum (*21*, *22*), trigger events leading to cellular transformation, tumorigenesis, and enhanced cell motility (*23*). An understanding of the interaction of the IGFBPs with IGF-1 is a key starting point toward the generation of novel therapeutics aimed at inhibiting IGF signaling.

The solution structure of IGF-1 reveals the presence of two distinct binding domains, an IGF-1R-binding domain and an IGFBP-binding domain [Figure 1; (*24*)]. The primary structure of IGF-1 can be subdivided into four regions (A−D), which are based on sequence similarity to insulin (*25*). A form of IGF-1 that lacks the three N-terminal amino acids, des(1−3) IGF-1, has decreased affinity for the IGFBPs and, as a result, approximately 10−100 times greater biological activity at the IGF-1R than native IGF-1 (*26*). Competition binding data using site-directed mutants of IGF-1 suggest that residues 3−4, 15−16, and 49−51 are important in binding to the IGFBPs (*27*, *28*). The NMR structure demonstrates that N-terminal residues 1−3 and A-region residues 49−51 are in close proximity in three-dimensional space, thereby confirming the location and structure of the IGFBP-binding domain on IGF-1 (left of Figure 1). Of the three N-terminal residues within the IGFBP-binding domain, Glu 3 is the most significant. The Gly 1 residue has been shown not to be essential for binding (*29*) but provides a key site for chemical modification for studies of IGFBP-binding domain interactions (*30*).

Site-directed mutagenesis at positions 23, 24, and 25 of IGF-1 has revealed the involvement of this tripeptide in IGF-1R and insulin receptor (IR) binding (*31*). NMR data has confirmed the presence of a cleft made up of Phe 23, Tyr 24, Phe 25, Val 44, and Arg 21 (*24*). Maly and Luthi (*32*) reported that Tyr 24, 31, and 60 were protected from iodination when IGF-1 was bound to its receptor, indicating the importance of these residues in contacting the IGF-1R. Cooke et al. (*24*) suggested that Tyr 31 and 60 are involved in maintaining the correct position of the IGF-1R binding cleft. When taken together, NMR and functional studies confirm the existence of a topologically distinct IGF-1R-binding domain within IGF-1, located on the opposite face from the IGFBP-binding domain (right of Figure 1).

The IGF-binding domain(s) on the IGFBPs have not been fully defined. The N and C termini are cysteine-rich, containing 8−9 intradomain disulfide bonds, and maintain a high degree of homology across the six IGFBPs; the mid-region is more variable (*18*). The conservation of these regions, as well as structure−function studies to date, implicate the participation of both the N- and C-terminal domains in IGF-1 binding. It has been observed that IGFBP-2 and IGFBP-3 possess different structural requirements for IGF binding. Several groups have shown that the N terminus of IGFBP-3 and IGFBP-5 is an important binding determinant (*33*−*36*). Conversely, the C terminus of IGFBP-2 has been shown to play a role in IGF binding (*37*−*39*). Furthermore, recent studies have indicated a requirement for both the N and C termini of IGFBP-2, IGFBP-3, and IGFBP-5 in IGF binding (*40*−*42*). Our present findings provide additional evidence for a mechanism by which IGFBP-2 and IGFBP-3 bind both faces of IGF-1.

To date, methodology used to characterize the structural basis for IGFBP inhibition of IGF action include mutagenesis, NMR, X-ray crystallographic, and IGFBP fragment analyses. Given that perturbations in the N terminus could adversely impact the binding interactions occurring in the C terminus and vice versa, mutagenesis studies must be interpreted with caution. The lack of X-ray crystallographic or NMR analyses of intact IGFBPs alone or complexed with IGF-1 has further limited our understanding of the precise contact sites involved in high-affinity binding. To address this paucity, we have synthesized and characterized three selectively monobiotinylated isoforms of IGF-1 for use in binding, ligand blotting, and BIAcore analyses. Our findings demonstrate the contribution of both the IGFBP-binding domain and IGF-1R-binding domain on IGF-1 in binding to IGFBP-2 and IGFBP-3. In addition, the data presented here highlight the utility of biotinylated IGF-1 in place of $^{125}$I-IGF-1 for ligand blotting.

## EXPERIMENTAL PROCEDURES

*Materials*. Recombinant human IGF-1 was provided by Genentech (South San Francisco, CA). EZ-Link NHS-Biotin, EZ-Link NHS-LC-Biotin, NeutrAvidin-peroxidase, and tris-(2-carboxyethylyl)phosphine hydrochloride were obtained from Pierce (Rockford, IL). The HPLC column (Discovery BIO Wide Bore $C_{18}$, 25 cm × 4.6 mm, 5 $\mu$m) was obtained from Supelco (Bellefonte, PA). Trypsin and pepsin was obtained from Worthington Biochemical Corporation (Freehold, NJ). Recombinant human IGFBP-3 (N109D) (*33*) of bacterial origin was obtained from Upstate, Inc. (Charlottesville, VA). Recombinant human IGFBP-2 was purified from DHFR$^-$ Chinese hamster ovary cells (*43*) stably transfected with pCMV-hIGFBP-2 and pMT2 containing murine dihydrofolate reductase, as described previously (*30*). cDNA encoding human IGFBP-2 was obtained from Dr. Jörg Landwehr (Hoffman-La Roche, Basel, Switzerland). All other materials were of reagent grade or higher.

*Synthesis and Purification of Biotinylated IGF-1*. IGF-1 (0.5 mg, 65 nmol) was dissolved in 25 $\mu$L of 0.1 M acetic

acid and 975 μL of 0.1 M sodium phosphate buffer (pH 7.4). To generate mono-, di-, tri-, and tetrabiotinylated IGF-1, a 2.5-fold molar excess of EZ-Link NHS-Biotin (162.5 nmol/100μL) was reacted with IGF-1 at 23 °C for 15−20 min. Generation of the monobiotinylated forms of IGF-1 was favored by reaction of IGF-1 with an equimolar amount of EZ-Link NHS-Biotin or EZ-Link NHS-LC-Biotin at 23 °C for 9 min, respectively. Unreacted ester was quenched by the addition of 4 μL of 2 M Tris at pH 7.4, and the reaction mixtures were dried in vacuo in a SpeedVac concentrator (Savant Instruments, Inc., Farmingdale, NY). The lyophilized mixture was dissolved in 300 μL of 50 mM triethanolamine phosphate (pH 3) containing 20% acetonitrile and 10 μL of 100% trifluoroacetic acid and injected onto a $C_{18}$ column equilibrated in 50 mM triethanolamine phosphate (pH 3) and 15% acetonitrile at a flow rate of 1 mL/min. After 10 min, IGF-1 and the reaction products were eluted with a linear gradient of 15−36% acetonitrile developed over 65 min. Individual peaks were collected, dried, dissolved in 500 μL of 0.1% trifluoroacetic acid and 10 μL of 100% trifluoroacetic acid, and reinjected onto a $C_{18}$ column equilibrated in 24% acetonitrile and 0.1% trifluoroacetic acid. After 10 min, the IGF-1 (native and biotinylated) was eluted with a gradient of 24−48% acetonitrile over 45 min. The major peak from each run was collected, dried, and stored at −20 °C until further analysis. All biotinylated forms of IGF-1 are stable when stored in dry form at −20 °C for at least one year.

*Trypsin Digestion of IGF-1*. Native and monobiotinylated IGF-1 (100 μg) was solubilized in $dH_2O$, 1.5 M Tris at pH 8.7, and *n*-propanol (200 μL each) and reduced and alkylated by incubation with tris(2-carboxyethylyl)phosphine hydrochloride (2 mg) and 4-vinyl pyridine (2 μL) (*44*). Alkylated samples (100 μg) were dried and digested with trypsin at an enzyme/substrate ratio of 1:10 for 3 h at 37 °C in 30 μL of $dH_2O$ plus 160 μL each of 0.1 M 4-ethylmorpholine (pH 8.5) and 1.5 M Tris (pH 8.7) (*45*). A fresh aliquot of trypsin was then added, and the digestion continued overnight. Samples were dried and injected onto a $C_{18}$ column equilibrated in 0.1% trifluoroacetic acid. Tryptic fragments were eluted with a linear gradient of 0−60% acetonitrile over 90 min. Peaks representing individual fragments were collected, dried, and analyzed by MALDI−TOF MS.

*MALDI−TOF MS*. Intact native, mono-, di-, tri-, and tetrabiotinylated IGF-1 and tryptic digests of native IGF-1 and two of the monobiotinylated species were analyzed by MALDI−TOF MS. Dried HPLC fractions (1 μg) were dissolved in 60% acetonitrile containing 0.1% trifluoroacetic acid (5 μL). Aliquots (0.5 μL) of each fraction were mixed with the matrix, 50 mM α-cyano-4-hydroxycinnamic acid (1.5 μL). A stainless steel sample plate was spotted with the matrix alone (0.5 μL) and air-dried. Aliquots (0.5 μL) of the sample mixtures were then spotted on top of the dried matrix. The samples were analyzed using an ABI Voyager-DE MALDI−TOF mass spectrometer equipped with a 337-nm nitrogen laser (Applied Biosystems, Foster City, CA). A delayed extraction source was operated in linear mode (1.2-m ion flight path and 25-kV accelerating voltage), yielding an instrumental resolution of ∼700 (full width at half-maximum) at *m*/*z* 1297.51 Da. One mass spectrum was based on the average of 250 mass scans. External calibration was performed using angiotensin I (1297.51 Da), thioredoxin (11 674.48 Da) and bovine insulin (5734.59 Da) as the standards. Mass accuracy was ±0.1%.

*Pepsin Digestion of Native IGF-1*. IGF-1 and $N^{\epsilon Lys65/68b}$-IGF-1 (50 μg) were digested with pepsin in an enzyme/substrate ratio of 1:10 for 4 h at 23 °C in 0.01 M HCl (100 μL) (*46*). Samples were dried and injected onto a $C_{18}$ column equilibrated in 0.1% trifluoroacetic acid. Peptic fragments were eluted in a linear gradient of 0−36% acetonitrile over 75 min. Peaks representing individual fragments were collected, dried, and analyzed by MALDI−TOF MS. Peaks corresponding to fragments of IGF-1 containing Lys 65 and Lys 68 were analyzed further by MALDI−TOF−TOF MS. For MALDI−TOF−TOF MS, dried HPLC fractions (1 μg) were dissolved in 60% acetonitrile containing 0.1% trifluoroacetic acid (5 μL). Aliquots (0.5 μL) of each sample were mixed with the matrix, 50 mM α-cyano-4-hydroxycinnamic acid (1.5 μL). Aliquots (0.5 μL) of the sample mixtures were then spotted onto a stainless-steel sample plate and air-dried. Samples were analyzed using an Applied Biosystems 4700 Proteomics Analyzer with TOF/TOF optics (Applied Biosystems), for sequencing of peptic fragments. External calibration was performed using angiotensin I (1296.685 Da), des-arg1-bradykinin (904.468 Da), and glu1-fibrinopeptide (1570.677 Da). Mass accuracy was ±0.005%.

*Solid-Phase-Binding Analysis of Biotinylated IGF-1*. Polystyrene tubes (12 × 75 mm) were coated with rhIGFBP-2 or rhIGFBP-3 (4 ng/tube) in 0.2 M sodium borate (200 μL at pH 9.2) at 23 °C for 2.5 h. Coated tubes were washed and blocked with 1% bovine serum albumin (BSA) in 300 μL of assay buffer (50 mM HEPES (pH 7.4), 0.15 M NaCl, 0.05% $NaN_3$, and 0.1% Tween-20) and stored at 4 °C in 0.3% BSA in 300 μL of assay buffer. $^{125}$I-IGF-1 (15 000−20 000 cpm, 10 nCi; Amersham Biosciences, Piscataway, NJ) plus various concentrations of unlabeled IGF-1 (50 fM−500 nM) were added to each tube. After 4 h at 23 °C, the buffer containing free IGF-1 was aspirated and the tubes were washed 1 time with 0.3% BSA in 300 μL of assay buffer and 2 times with 300 μL of assay buffer. Specifically bound $^{125}$I-IGF-1 was quantified in a Compugamma spectrometer (LKB−Wallac, Turku, Finland). Counts detected in the presence of 500 nM IGF-1 (nonspecific binding) were subtracted to obtain specific binding. $EC_{50}$ values were calculated using the equation $B = B_{max}/(1 + [\text{ligand}]/IC_{50})$, where $B$ is the concentration of bound ligand and $B_{max}$ is the maximal binding observed. Prism version 4 (GraphPad Software, Inc., San Diego, CA) was used to minimize the sum of the squares of the differences from the mean $EC_{50}$ values for each concentration of IGF-1. The calculated $EC_{50}$ values were used to generate smooth curves. Assays were conducted with native IGF-1 and monobiotinylated IGF-1 using both rhIGFBP-2 and rhIGFBP-3 coated tubes. Assays were conducted with triplicate concentrations and repeated at least 3 times.

*Ligand Blotting Using Biotinylated IGF-1*. rhIGFBP-2 or rhIGFBP-3 was combined with SDS sample buffer (62.5 mM Tris (pH 6.8), 2% SDS, 5 mM EDTA, 0.05 mg/mL bromophenol blue, and 7.5% sucrose) without dithiothreitol and resolved on a 12.5% SDS−polyacrylamide gel according to the procedure of Laemmli (*47*) using a Hoefer Scientific Instruments (San Francisco, CA) gel apparatus. Proteins were transferred to nitrocellulose membranes (Osmonics Inc.,

Westborough, MA) using a Semi-Phor (Hoefer Scientific Instruments) transfer apparatus. The membrane was washed with TBS (10 mM Tris-HCl (pH 7.4) and 150 nM NaCl) containing 3% Triton-X-100 for 10 min. The nitrocellulose was quenched with 0.2% gelatin in TBS for 1 h at 23 °C and then washed with TBST (TBS containing 0.1% Tween-20) for 5 min. The nitrocellulose was then incubated with the indicated biotinylated IGF-1 (10 ng/mL or as indicated) in TBST containing 0.5% BSA overnight at 4 °C. The blot was washed with 0.2% gelatin in TBS (3× for 10 min each) and incubated with NeutrAvidin-peroxidase (1$\mu$g/$\mu$L) in TBST containing 0.5% BSA for 1 h at 23 °C. The blot was then washed with 0.2% gelatin as described above, and rhIGFBPs were detected using enhanced chemiluminescence (Amersham Biosciences). Blots were exposed to Kodak Biomax MR film for 1−30 min and developed using a Konica SRX-101 film developer.

*Ligand Blotting Using $^{125}$I-IGF-1*. rhIGFBP-2 and rhIGFBP-3 samples were prepared and resolved on 12.5% SDS−polyacrylamide gels and transferred to nitrocellulose as described above. Ligand blots using $^{125}$I-IGF-1 iodinated on Tyr 31 (Amersham Biosciences) were performed according to Hossenlopp et al. (*48*) and Horney et al. (*49*). Briefly, nitrocellulose membranes were washed with TBS containing 3% Triton-X for 30 min at 4 °C, followed by TBS containing 1% BSA for 2 h at 4 °C and finally in TBST for 10 min at 4 °C. The membrane was then incubated with 100 000 cpm/mL of $^{125}$I-IGF-1 in TBST containing 1% BSA overnight at 4 °C. The blot was then washed twice with TBST for 30 min at 4 °C and 3 times with TBS for 30 min at 4 °C, exposed to Kodak Biomax MR film for 2−3 weeks at −80 °C, and developed using a Konica SRX-101 film developer.

*Analysis of IGFBPs from Conditioned Medium*. SV40 transformed murine mesangial cells (ATCC, Manassas, VA) were grown to confluence in a 3:1 mixture of Dulbecco's modified Eagle's medium: F12 Ham medium supplemented with 5% fetal bovine serum (FBS) and penicillin (100 units/mL)−streptomycin (100 $\mu$g/mL) at 37 °C in an atmosphere of 95 and 5% $CO_2$ in a humidified incubator. At confluence, growth medium was removed and serum-free medium was added for 24 h. Concurrently, human ARPE-19 retinal pigment epithelium cells (ATCC) were grown to confluence in RPMI-1640 medium supplemented with 10% FBS in the conditions described above. At confluence, growth medium was removed and replaced with serum-free medium containing 100 nM IGF-1 for 12 h. Conditioned media (CM) was then collected from both cell lines and centrifuged for 15 min at 2500 rpm to remove cell debris. The supernatants were incubated with 10% final trichloroacetic acid for 12 h at 4 °C to precipitate the IGFBPs. The samples were then centrifuged at 14 000 rpm for 5 min at 4 °C. The pellets were washed with cold acetone (100%) and recentrifuged. SDS-sample buffer was added to the pellets, which were then resolved on a 12.5% SDS−polyacrylamide gel. The proteins were then transferred to nitrocellulose and blotted with either monobiotinylated IGF-1 or $^{125}$I-IGF-1 as indicated.

*BIAcore Analysis: Biosensor Surface Preparation*. Biosensor studies were performed on a BIAcore 3000 instrument (BIAcore, Inc.; Piscataway, NJ). Monobiotinylated forms of IGF-1 ($N^{\epsilon Lys27b}$-IGF-1, $N^{\alpha Gly1b}$-IGF-1, and $N^{\epsilon Lys65/68b}$-IGF-1) were captured on individual flowcells of a streptavidin (SA)-coated BIAcore SA sensor chip in the amounts of ∼200 response units (RU), respectively. Ligands were diluted to 1 $\mu$g/mL in HBS buffer (10 mM HEPES and 150 mM NaCl at pH 7.4) and injected at 5 $\mu$L/min until the desired response units were captured. To correct for refractive index changes, nonspecific binding, and instrument drift, a reference flowcell contained the SA-coated surface only. All experiments were performed at 25 °C.

*Acquisition of Kinetic Binding Data.* Analytes, IGFBP-2 (1.95, 3.9, 7.8, 15.63, 31.25, 62.5, 125, and 250 nM) and IGFBP-3 (3.9, 7.8, 15.63, and 62.5 nM), were diluted to 1 $\mu$g/mL in HBS and injected during the association phase for 5 min (50 $\mu$L/min) using the kinject command. HBS alone was perfused (10 min) during the dissociation phase. The biosensor surface was regenerated with 0.01 M NaOH. Each sensorgram shown is representative of two separate experiments run in duplicate, with the reference cell values subtracted. BIAevaluation software version 3.1 (BIAcore Inc.) was used to fit the data, utilizing the Langmuir 1:1 binding model and the global data analysis option.

## RESULTS

*Synthesis and Characterization of Biotinylated IGF-1*. IGF-1 contains four possible sites of derivatization with NHS-biotin, the $\epsilon$-amino groups of 3 lysyl residues at positions 27, 65, and 68 and the α-amino group of the N-terminal glycine. Significantly, Gly 1 is contiguous with the IGFBP-binding domain, while Lys 27 is in close proximity to the IGF-1R-binding domain. Lys 65 and Lys 68 are outside of these domains (see Figure 1). To favor generation of monobiotinylated isoforms of IGF-1, we altered the ratio of NHS-biotin to IGF-1. A 2.5-fold molar excess of NHS-biotin (Figure 2 A) yielded nine distinct products as well as unreacted IGF-1, while a 1:1 molar ratio of NHS-biotin/IGF-1 (Figure 2B) resulted in only three major products. The elution profiles obtained were consistent with those observed by Horney et al. (*30*) and Yip et al. (*50*). MALDI−TOF MS analysis of the individual peaks in both elution profiles indicated the presence of underivatized IGF-1 (peaks labeled I only) with an observed mass of 7654.6 Da (Figure 3A, predicted average mass of 7654.7 Da), three monobiotinylated products (peaks labeled M1−M3 only) (Figure 3B, observed mass of 7874.2 ± 0.3 Da and predicted average mass of 7879.7 Da), and three dibiotinylated products (peaks labeled D only) with an observed mass of 8099.2 ± 0.8 Da (Figure 3C, predicted average mass of 8104.7 Da). Elution profile 2A also contained two tribiotinylated products (peaks labeled T only) with an observed mass of 8320.7 ± 0.1 Da (Figure 3D, predicted average mass of 8329.7 Da) and one tetrabiotinylated derivative (peak labeled Q only) with an observed mass of 8548.3 Da (Figure 3E, predicted average mass of 8554.7 Da).

Figure 4 summarizes mass spectrometric analyses of tryptic digests of two of the monobiotinylated derivatives (M1 and M3) and a peptic digest of M2 to verify the location of the biotin within each derivative. Figure 4A depicts the tryptic and peptic cleavage sites on IGF-1 and the resulting fragments generated. MALDI−TOF MS analysis of tryptic fragments of M1 and M3, in comparison with native IGF-1, indicated that peak M1 corresponded to $N^{\epsilon Lys27b}$-IGF-1 based on the observed mass of fragment $B_T$ (1896.4 Da), while peak M3 contains $N^{\alpha Gly1b}$-IGF-1 based on the observed mass

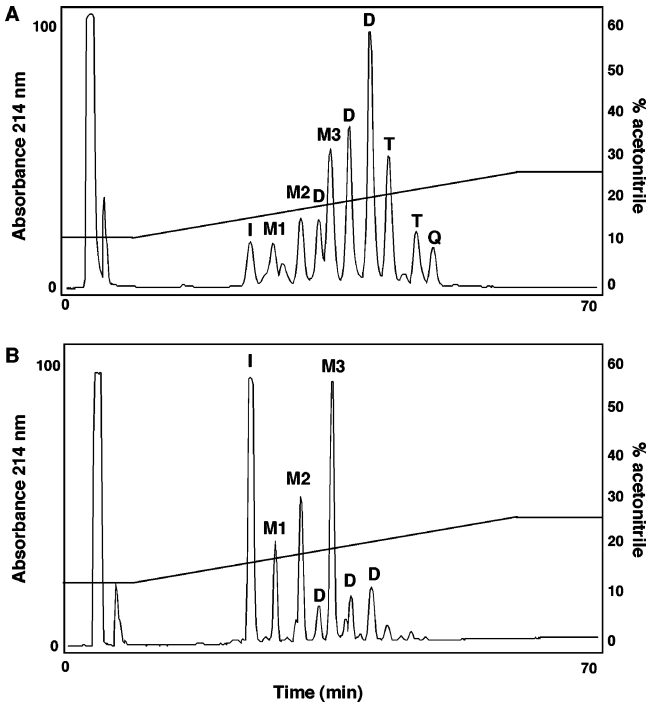


FIGURE 2: Synthesis of biotinylated IGF-1. IGF-1 has four possible sites of derivatization with NHS-biotin, lysine residues 27, 65, and 68, as well as the N-terminal glycine. NHS-biotin was reacted with IGF-1 in a (A) 2.5:1 molar ratio or (B) 1:1 molar ratio. Reaction products were dried and separated using RP-HPLC on a $C_{18}$ column in an acetonitrile gradient. Individual peaks were collected and further purified in a second round of RP-HPLC. Reaction products included (A) mono- (M1−M3), di- (D), tri- (T), tetrabiotinylated (Q), and native IGF-1 (I) or (B) mono- and dibiotinylated IGF-1, as well as native IGF-1.

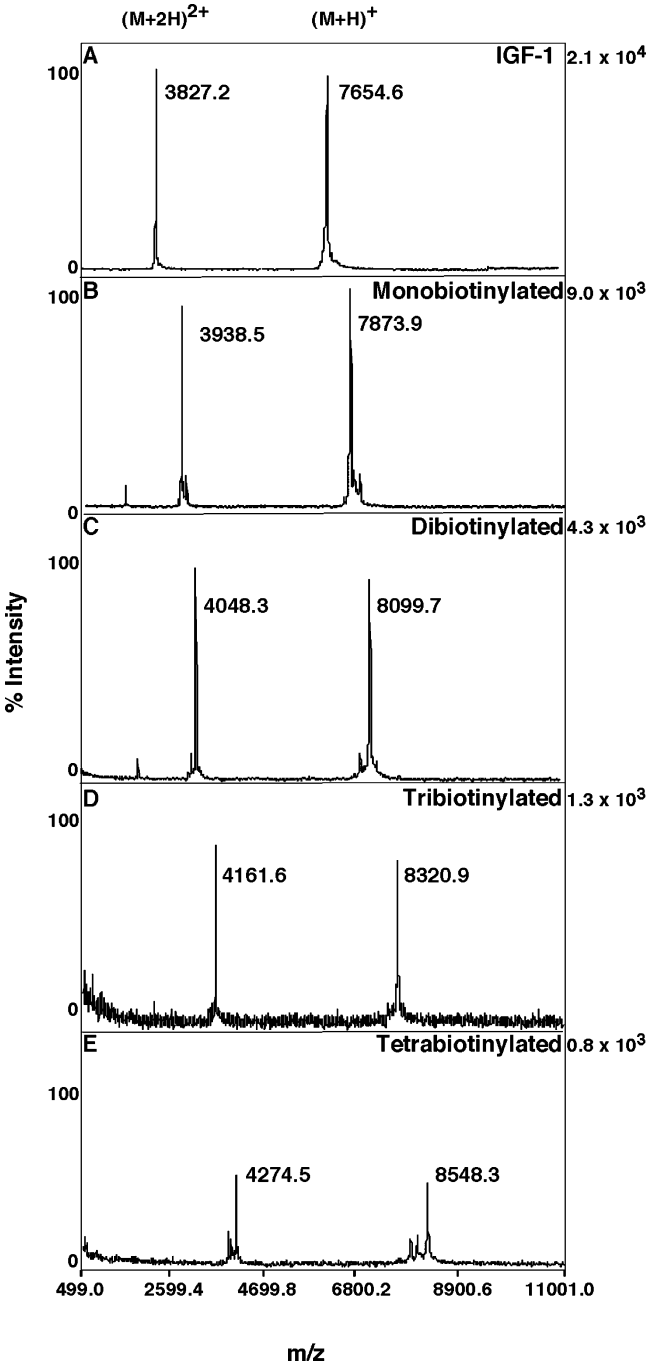


FIGURE 3: MALDI−TOF MS analysis of biotinylated IGF-1. MALDI−TOF MS analysis was performed on RP-HPLC-purified fractions to confirm derivatization with NHS-biotin. Addition of a single biotin moiety corresponds to a mass shift of 225 Da (NHS-biotin). The spectra shown compare native IGF-1 with mono-, di-, tri-, and tetrabiotinylated IGF-1 synthesized using NHS-biotin.

of fragment $A_T$ (2631.5 Da) (parts A and B of Figure 4). In each case, MALDI−TOF MS analysis of these peaks confirmed that no other tryptic fragments were biotinylated because their *m*/*z* ratios were in agreement those of native IGF-1 (data not shown). Because the Lys 65 and Lys 68 containing tryptic fragment ionized poorly during MALDI−TOF MS analysis, pepsin digestion was carried out to obtain a fragment with improved ionization properties. Pepsin digestion was performed on unreduced native IGF-1 (data not shown) and M2-IGF-1. The $C_P$−$D_P$ peptide from M2-IGF-1, which contains one disulfide bond, was isolated and analyzed by MALDI−TOF−TOF MS. The MALDI−TOF mass spectrum indicated that the disulfide bond connecting fragments $C_P$ and $D_P$ was broken during ionization in the mass spectrometer. Subsequently, the ion corresponding to $D_P$ (*m*/*z* 1374.6 Da, data not shown), which is composed of residues 60−70, was selected, and a tandem mass spectrum was acquired (Figure 4C). Analysis of the b and y ions of $D_P$ demonstrated that M2-IGF-1 was a mixture of two monobiotinylated derivatives of IGF-1, one biotinylated at Lys 65 and one at Lys 68 ($N^{\epsilon Lys65/68b}$-IGF-1). Specifically, ions $b_6$ and $y_5$, which contain only Lys 65 or Lys 68, respectively, were observed in both the underivatized and biotinylated forms, indicating the presence of two distinct biotinlyated species of IGF-1 within the M2-IGF-1 HPLC peak. This finding also serves to explain why only three HPLC peaks corresponding to monobiotinylated species were observed (Figure 2) despite the presence of four predicted sites of biotinylation within IGF-1.

The effect of selective biotinylation of IGF-1 on its affinity for IGFBP-2 and IGFBP-3 was examined using a competitive solid-phase-binding assay (Figure 5). In this assay, IGFBP-2 or IGFBP-3 was immobilized on polystyrene tubes (4 ng per tube) and the ability of biotinylated IGF-1 to compete with $^{125}$I-IGF-1 was assessed. These data indicated that $N^{\alpha Gly1b}$-IGF-1 and $N^{\epsilon Lys65/68b}$-IGF-1 exhibited a reduced affinity for IGFBP-2, while $N^{\epsilon Lys27b}$-IGF-1 and $N^{\epsilon Lys65/68b}$-IGF-1 exhibited a reduced affinity for IGFBP-3 compared with native IGF-1. However, a dramatic loss of binding was not observed. The $EC_{50}$ values for IGFBP-2 binding of IGF-

A

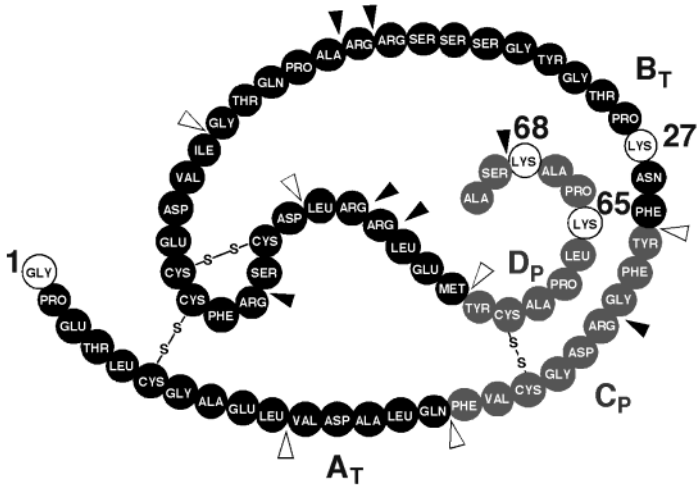


B

| HPLC peak | Fragment | Underivatized m/z | Biotinylated m/z | Observed m/z | Biotinylated Residue |
|---|---|---|---|---|---|
| **M3** | $A_T$ | 2404.8 | 2631.2 | **2631.5** | **Gly-1** |
| **M1** | $B_T$ | 1668.8 | 1895.1 | **1896.4** | **Lys-27** |
| **M2** | $D_P$ | 1148.3 | 1374.3 | **1374.6** | **Lys-65/68** |

C

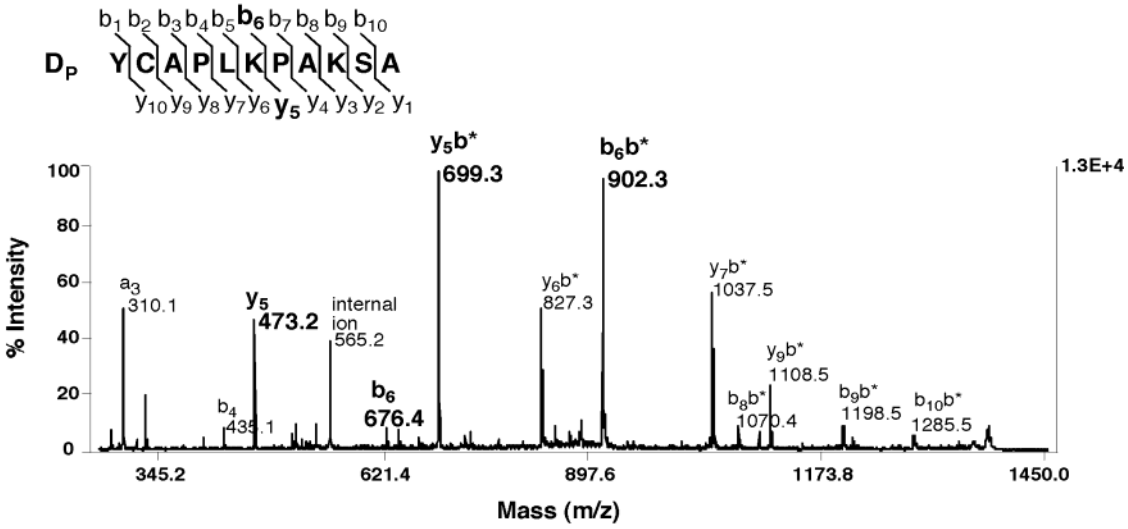


FIGURE 4: Identification of the sites of biotinylation within the monobiotinylated derivatives of IGF-1. (A) Primary sequence of IGF-1 is shown. Filled arrowheads indicate trypsin cleavage sites, and open arrowheads indicate pepsin cleavage sites. $A_T$ and $B_T$ indicate tryptic fragments, while $C_P-D_P$ indicates a peptic fragment (shaded in gray). (B) *m*/*z* of the biotinylated fragment observed for each derivative was compared with the predicted *m*/*z* of the corresponding fragment, unmodified and biotinylated, in the table provided. The *m*/*z* of the remaining fragments were consistent with unmodified IGF-1 fragments (data not shown). These data indicated that RP-HPLC peak M1 corresponds to $N^{\epsilon Lys27b}$-IGF-1 and M3, to $N^{\alpha Gly1b}$-IGF-1. (C) Tandem mass spectrum of the $D_P$ fragment indicated that peak M2 is composed of a mixture of $N^{\epsilon Lys65b}$-IGF-1 and $N^{\epsilon Lys68b}$-IGF-1. Ions labeled with b* indicate biotinylated ions.

1, $N^{\epsilon Lys27b}$-IGF-1, $N^{\alpha Gly1b}$-IGF-1, and $N^{\epsilon Lys65/68b}$-IGF-1 were 137, 153, 237, and 240 pM, respectively (Figure 5A). For IGFBP-3 binding to IGF-1, $N^{\epsilon Lys27b}$-IGF-1, $N^{\alpha Gly1b}$-IGF-1, and $N^{\epsilon Lys65/68b}$-IGF-1, the $EC_{50}$ values were 64, 178, 91, and 183 pM, respectively (Figure 5B).

*Ligand Blot Analysis Using Selectively Monobiotinylated IGF-1*. The utility of the monobiotinylated IGF-1 derivatives as IGFBP detection reagents was assessed in ligand blot assays. Because ligand blotting assays do not detect low affinity interactions or enable quantification of slight differences in IGF-1/IGFBP affinities, one might expect equivalent ligand blotting efficiencies for all monobiotinylated IGF-1 species. Increasing amounts of recombinant IGFBP-2 and IGFBP-3 (5, 10, and 20 ng) were resolved on 12.5% polyacrylamide gels under nonreducing conditions, transferred to nitrocellulose, and probed with each monobiotinylated IGF-1 derivative (prepared with NHS-biotin) as well as tetrabiotinylated-IGF-1 (QB-IGF-1) using NeutrAvidin-

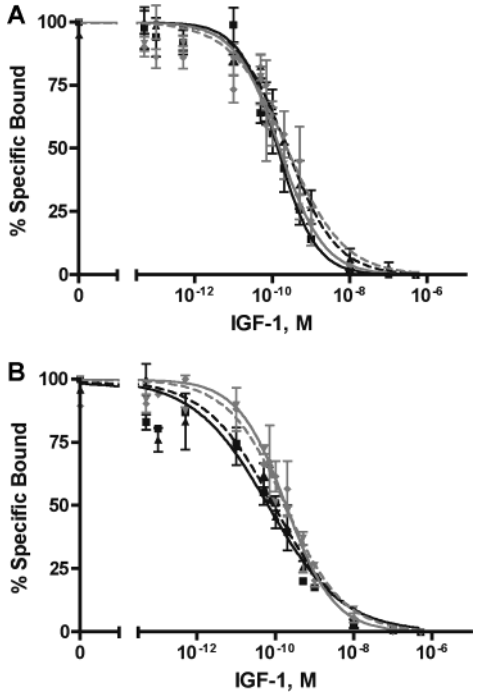


FIGURE 5: Solid-phase-binding analysis of monobiotinylated IGF-1. Affinities of native and biotinylated IGF-1 for IGFBP-2 and IGFBP-3 were compared in competitive solid-phase-binding assays. IGFBP-2- and IGFBP-3-coated polystyrene tubes (4 ng/tube) were incubated with test ligand and 15 000−20 000 cpm $^{125}$I-IGF-1 as the tracer. (A) $EC_{50}$ values for IGFBP-2 binding of IGF-1 (■, —), $N^{\epsilon Lys27b}$-IGF-1 (▼, —), $N^{\alpha Gly1b}$-IGF-1 (▲, - - -), and $N^{\epsilon Lys65/68b}$-IGF-1 (◆, - - -) were 137, 153, 237, and 240 pM, respectively. (B) For IGFBP-3 binding to IGF-1 (■, —), $N^{\epsilon Lys27b}$-IGF-1 (▼, —), $N^{\alpha Gly1b}$-IGF-1 (▲,- - -), and $N^{\epsilon Lys65/68b}$-IGF-1 (◆, - - -), the $EC_{50}$ values were 64, 178, 91, and 183 pM. $EC_{50}$ values were generated using Prism version 4.0 software. Data points shown are the average values of three independent experiments performed in triplicate. Binding curves were generated as described under the Experimental Procedures.

peroxidase to detect the biotin moiety (Figure 6). As shown in the first and second sets of three lanes, QB-IGF-1 and $N^{\epsilon Lys65/68b}$-IGF-1 demonstrated equivalent, robust labeling of IGFBP-2 and IGFBP-3, while $N^{\alpha Gly1b}$-IGF-1 and $N^{\epsilon Lys27b}$-IGF-1 (lanes 7−12) exhibited negligible labeling. On the basis of competition binding assays (Figure 5) demonstrating nearly equivalent binding affinities for the monobiotinylated species, the decreased labeling observed in ligand blotting could not be explained by altered binding affinities. To verify $N^{\alpha Gly1b}$-IGF-1 and $N^{\epsilon Lys27b}$-IGF-1 were binding to IGFBP-2 and IGFBP-3 on the nitrocellulose and that the lack of a signal was due to the biotin being sequestered, a competition binding experiment was conducted using recombinant IGFBP-2 and IGFBP-3. As shown in Figure 7, ligand blotting was performed with $N^{\epsilon Lys65/68b}$-IGF-1 (5 ng/mL) alone, $N^{\alpha Gly1b}$-IGF-1 alone (30 ng/mL), and a combination of $N^{\epsilon Lys65/68b}$-IGF-1 (5 ng/mL) and $N^{\alpha Gly1b}$-IGF-1 (30 ng/mL). A duplicate experiment was performed using $N^{\epsilon Lys27b}$-IGF-1 in place of $N^{\alpha Gly1b}$-IGF-1. In each case, addition of $N^{\epsilon Lys27b}$-IGF-1 or $N^{\alpha Gly1b}$-IGF-1 significantly reduced the ability of $N^{\epsilon Lys65/68b}$-IGF-1 to label the IGFBPs, confirming that $N^{\epsilon Lys27b}$-IGF-1 and $N^{\alpha Gly1b}$-IGF-1 were competing for binding to IGFBP-2 and IGFBP-3.

We next assessed the effectiveness of the monobiotinylated IGF-1 species in detecting IGFBPs in CM. As observed with the recombinant binding proteins, native IGFBP-2 and IGFBP-3 from CM exhibited the same differential staining with $N^{\epsilon Lys65/68b}$-IGF-1 versus $N^{\alpha Gly1b}$-IGF-1 and $N^{\epsilon Lys27b}$-IGF-1 (Figure 8). $N^{\epsilon Lys65/68b}$-IGF-1 and $^{125}$I-IGF-1 demonstrated equivalent, strong labeling of IGFBP-2 and IGFBP-3 from CM, while negligible labeling was observed with $N^{\alpha Gly1b}$-IGF-1 and $N^{\epsilon Lys27b}$-IGF-1. As expected, murine IGFBP-2, which is 18 residues shorter than human IGFBP-2, ran faster than human IGFBP-2 (lanes labeled CM in Figure 8A), and three primary species of IGFBP-3 are detectable in CM (Figure 8B) from human ARPE-19 cells, representing differentially N-glycosylated forms at each of its three consensus sites of glycosylation (*51*). These data, in combination with the solid-phase-binding results, suggest that the differential labeling observed in ligand blotting with $N^{\alpha Gly1b}$-IGF-1 and $N^{\epsilon Lys27b}$-IGF-1 was the result of these residues being in close contact with the IGFBPs, thus reducing the ability of NeutrAvidin-peroxidase to access the biotin moieties on Gly 1 and Lys 27.

*Ligand Blot Analysis Using LC-Monobiotinylated IGF-1.* Because the solid-phase-binding analysis clearly showed that monobiotinylated species retained high affinity for IGFBP-2 and IGFBP-3 and this was validated by ligand blot competition binding (Figure 7), the differential labeling seen in ligand blotting (Figure 6) suggested that, owing to their roles in binding to the IGFBPs, biotin moieties present on Gly 1 and Lys 27 are inaccessible to NeutrAvidin-peroxidase. To further test this possibility, IGF-1 was biotinylated with a long chain form of NHS-biotin (LC-biotin), having a linker arm length of 22.4 Å, to extend the biotin moieties away from IGF-1, relative to when NHS-biotin is attached (linker arm length of 13.5 Å). LC-biotin monobiotinylated derivatives of IGF-1 were synthesized and purified as described in the Experimental Procedures. Reaction of LC-biotin with IGF-1 in a 1:1 molar ratio resulted in an elution profile that was essentially identical to that observed with NHS-biotin (data not shown). Figure 9A shows MALDI−TOF MS analysis of a LC-biotin monobiotinylated derivative of IGF-1 (M1−M3; observed mass of 8002.9 ± 1.7 Da and predicted average mass of 8004.7 Da). LC-biotin was less reactive with IGF-1 than with NHS-biotin because tri- or tetrabiotinylated products were not observed even following the addition of a 2.5 or 5 molar excess of the long chain form of biotin. As shown in Figure 9B, extension of the biotin group in the $N^{\alpha Gly1}$(LC-biotin)-IGF-1 and $N^{\epsilon Lys27}$(LC-biotin)-IGF-1 derivatives increased the accessibility of NeutrAvidin-peroxidase binding, which translated into a more robust signal compared with that achieved with the NHS-biotin counterparts. The NHS-biotin and LC-biotin $N^{\epsilon Lys65/68b}$ derivatives demonstrated equivalent labeling of IGFBP-2 and IGFBP-3, consistent with Lys 65 and Lys 68 being uninvolved in the IGFBP interaction.

*BIAcore Analysis.* To validate the differential labeling pattern observed by ligand blot, we carried out BIAcore binding studies. $N^{\epsilon Lys27b}$-IGF-1, $N^{\alpha Gly1b}$-IGF-1, and $N^{\epsilon Lys65/68b}$-IGF-1 served as targets and were attached to individual flowcells of a SA-coated BIAcore sensor chip (203.67 ± 36.01 RU), while the 4th flowcell remained blank (control). IGFBP-2 and IGFBP-3 served as analytes and exhibited significant association with $N^{\epsilon Lys65/68b}$-IGF-1 (∼250 and ∼500 RU, respectively, Figure 10) compared with $N^{\epsilon Lys27b}$-IGF-1 or $N^{\alpha Gly1b}$-IGF-1 (0 and ∼50 RU, respectively). IGFBP-2 and

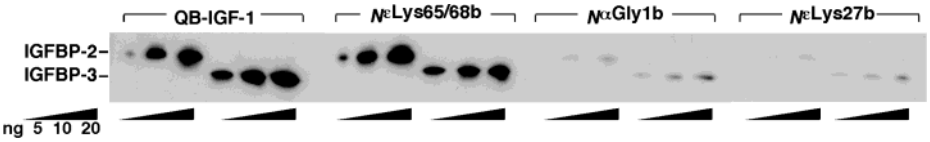


FIGURE 6: Ligand blot analysis of IGFBP-2 and IGFBP-3 using biotinylated IGF-1. IGFBP-2 and IGFBP-3 (5, 10, and 20 ng) were resolved on a 12.5% SDS−polyacrylamide gel under nonreducing conditions. The proteins were then transferred to a nitrocellulose membrane and blotted with the indicated species of biotinylated IGF-1. NeutrAvidin-peroxidase was added, and the IGFBPs were visualized using enhanced chemiluminesence. IGFBP-2 and IGFBP-3 were differentially labeled with QB-IGF-1 (1st set of lanes), $N^{\epsilon Lys65/68b}$-IGF-1 (2nd set of lanes), $N^{\alpha Gly1b}$-IGF-1 (3rd set of lanes), and $N^{\epsilon Lys27b}$-IGF-1 (4th set of lanes). The blot shown is representative of five independent experiments.

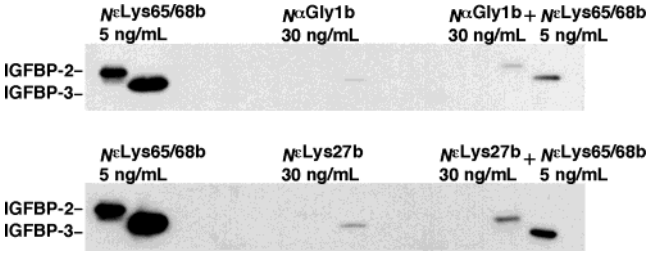


FIGURE 7: Competition of $N^{\epsilon Lys27b}$-IGF-1 and $N^{\alpha Gly1b}$-IGF-1 with $N^{\epsilon Lys65/68b}$-IGF-1 in ligand blot analysis of IGFBP-2 and IGFBP-3. IGFBP-2 and IGFBP-3 (20 ng) were resolved as described. Ligand blotting was performed with $N^{\epsilon Lys65/68b}$-IGF-1 (5 ng/mL) alone, $N^{\alpha Gly1b}$-IGF-1 alone (30 ng/mL), and a combination of $N^{\epsilon Lys65/68b}$-IGF-1 (5 ng/mL) and $N^{\alpha Gly1b}$-IGF-1 (30 ng/mL). A duplicate blot was developed using $N^{\epsilon Lys27b}$-IGF-1 in place of $N^{\alpha Gly1b}$-IGF-1. This showed that $N^{\epsilon Lys27b}$-IGF-1 and $N^{\alpha Gly1b}$-IGF-1 were able to compete against the $N^{\epsilon Lys65/68b}$-IGF-1 for binding to immobilized IGFBP-2 and IGFBP-3. The blot shown is representative of three independent experiments.

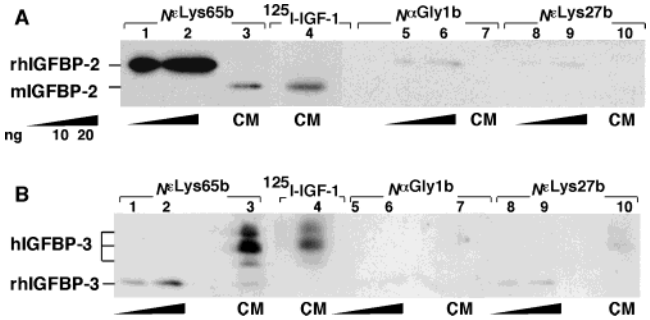


FIGURE 8: Ligand blot of conditioned medium from mesangial cells and retinal-pigment epithelial cells. (A) mIGFBP-2 from CM of SV40-transformed murine mesangial cells and (B) hIGFBP-3 from ARPE-19 human retinal-pigment epithelial cell CM were precipitated with trichloroacetic acid (10% final) and resolved on a 12.5% SDS−polyacrylamide gel under nonreducing conditions (lanes labeled CM). rhIGFBP-2 (10 and 20 ng; A, lanes 1, 2, 5, 6, 8, and 9) and rhIGFBP-3 (10 and 20 ng; B, lanes 1, 2, 5, 6, 8, and 9) standards were also resolved. The proteins were then transferred to nitrocellulose and blotted with the indicated species of biotinylated IGF-1 (A and B, lanes 1−3, 5−7, and 8−10) or $^{125}$I-IGF-1 (A and B, lane 4). The blot shown is representative of three independent experiments.

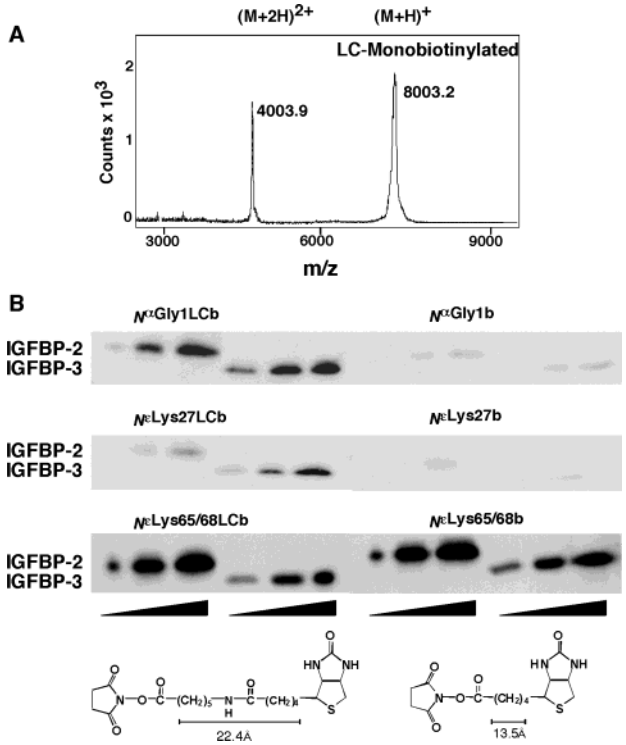


FIGURE 9: Ligand blot analysis of IGFBP-2 and IGFBP-3 using NHS-biotin versus NHS-LC-biotin derivatives of IGF-1. (A) MALDI−TOF MS spectrum of a monobiotinylated form of IGF-1 derivatized using LC-biotin. (B) IGFBP-2 and IGFBP-3 (5, 10, and 20 ng) were resolved on a 12.5% polyacrylamide gel under nonreducing conditions and blotted as described above. The IGFBPs were visualized by incubation with NHS-biotin derivatives or NHS-LC-biotin derivatives. $N^{\alpha Gly1b}$-IGF-1 and $N^{\epsilon Lys27b}$-IGF-1 exhibited modest labeling compared to $N^{\epsilon Lys65/68b}$-IGF-1 and QB-IGF-1. Increased labeling of IGFBP-2 and IGFBP-3 was observed with $N^{\alpha Gly1}$(LC-biotin)-IGF-1 and $N^{\epsilon Lys27}$(LC-biotin)-IGF-1 compared with the equivalent NHS-biotin derivatives. Similar labeling was observed with $N^{\epsilon Lys65/68b}$-IGF-1 and $N^{\epsilon Lys65/68}$(LC-biotin)-IGF-1. The blot shown is representative of three independent experiments.

IGFBP-3 exhibited rapid association with the $N^{\epsilon Lys65/68b}$-IGF-1 ($K_a = 1.66 \times 10^5$ and $1.68 \times 10^6$ M s$^{-1}$) surface using a 1:1 Langmuir binding model to fit the binding curves (parts A and C of Figure 10). The low $\chi^2$ values (<5.0) obtained indicate the satisfactory nature of this model. Conversely, IGFBP-2 had no detectable association with $N^{\epsilon Lys27b}$-IGF-1 or $N^{\alpha Gly1b}$-IGF-1 (data not shown), while the neglible amount of IGFBP-3 that interacted with $N^{\epsilon Lys27b}$-IGF-1 or $N^{\alpha Gly1b}$-IGF-1 demonstrated rapid association ($K_a = 1.66 \times 10^5$ and $1.68 \times 10^6$ M s$^{-1}$, respectively, Figure 10B). IGFBP-2 and IGFBP-3 exhibited similar, slow dissociation rates for $N^{\epsilon Lys65/68b}$-IGF-1 ($K_d = 6.24 \times 10^{-4}$ and $K_d = 3.11 \times 10^{-4}$ s$^{-1}$, respectively), reflecting the stable nature of these interactions (parts A and C of Figure 10). On the contrary, IGFBP-3 exhibited rapid dissociation kinetics from $N^{\epsilon Lys27b}$-IGF-1- and $N^{\alpha Gly1b}$-IGF-1-labeled biosurfaces ($1.07 \times 10^{-3}$ and $2.68 \times 10^{-3}$ s$^{-1}$, respectively) indicating unstable interactions (Figure 10B). IGFBP-3 also bound with 19.7-fold higher affinity to $N^{\epsilon Lys65/68b}$-IGF-1 ($K_d = 0.19$ nM) than IGFBP-2 ($K_d = 3.75$ nM). Finally, IGFBP-3 exhibited a 29.6- and 17-fold preference for $N^{\epsilon Lys65/68b}$-IGF-1 over $N^{\epsilon Lys27b}$-IGF-1 and $N^{\alpha Gly1b}$-IGF-1, respectively. BIAcore analysis thus confirmed the inaccessibility of Gly 1 and Lys 27 of IGF-1 when bound to IGFBP-2 and IGFBP-3. The observation that IGFBP-2 and IGFBP-3 preferentially associated with $N^{\epsilon Lys65/68b}$-IGF-1 over $N^{\epsilon Lys27b}$-IGF-1 and $N^{\alpha Gly1b}$-IGF-1 suggested that

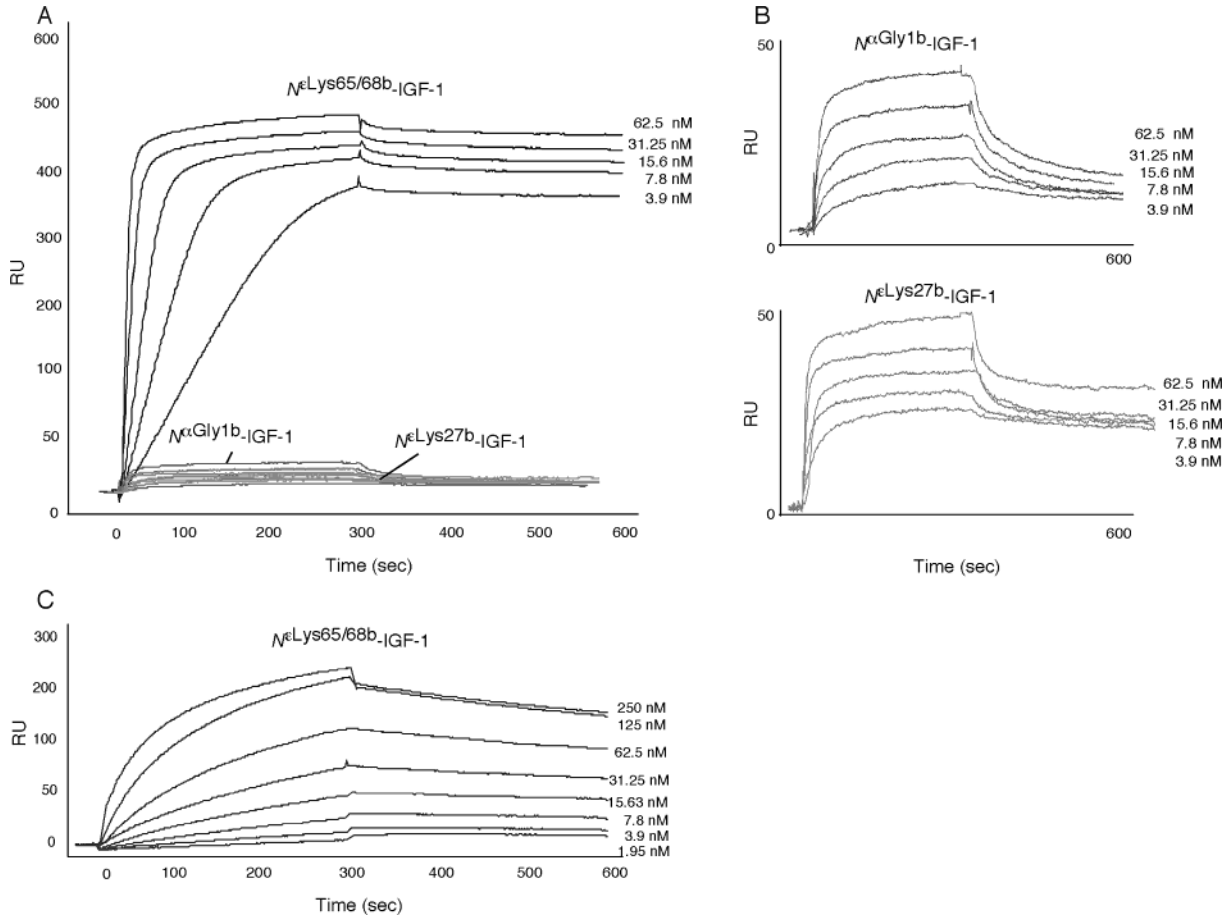


FIGURE 10: BIAcore analysis of IGFBP-2 and IGFBP-3 binding to monobiotinylated IGF-1. (A) IGFBP-3 binding to $N^{\epsilon Lys65/68b}$-IGF-1, $N^{\alpha Gly1b}$-IGF-1, and $N^{\epsilon Lys27b}$-IGF-1 derivatized flowcells of a SA sensor chip. (B) Enlarged view of IGFBP-3 binding to $N^{\alpha Gly1b}$-IGF-1- and $N^{\epsilon Lys27b}$-IGF-1-derivatized flowcells from A. (C) IGFBP-2 binding to $N^{\epsilon Lys65/68b}$-IGF-1-derivatized flowcell of a SA sensor chip. IGFBP-2 binding to $N^{\alpha Gly1b}$-IGF-1- and $N^{\epsilon Lys27b}$-IGF-1-derivatized flowcells was not detectable. Both IGFBP-2 and IGFBP-3 demonstrated a high-affinity, stable interaction with $N^{\epsilon Lys65/68b}$-IGF-1. Each sensorgram tracing is representative of two separate experiments run in duplicate, with the reference cell subtracted.

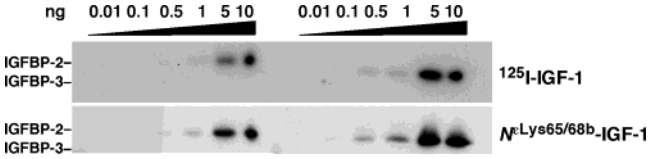


FIGURE 11: Ligand blot analysis using $^{125}$I-IGF-1 versus $N^{\epsilon Lys65/68b}$-IGF-1. IGFBP-2 and IGFBP-3 (0.01, 0.1, 0.5, 1, 5, and 10 ng) were resolved on a 12.5% polyacrylamide gel under nonreducing conditions. The proteins were then transferred to nitrocellulose and blotted with 100 000 cpm/mL $^{125}$I-IGF-1 or 10 ng/mL $N^{\epsilon Lys65/68b}$-IGF-1 as detailed in the Experimental Procedures. The $^{125}$I-IGF-1 blot was exposed to Kodak Biomax MR film for 2 weeks at −80 °C, while the $N^{\epsilon Lys65/68b}$-IGF-1 was incubated with NeutrAvidin-peroxidase followed by ECL reagent and exposed to film for 1−30 min. These ligand blot protocols demonstrated near equivalent labeling of IGFBP-2 and IGFBP-3. The blot shown is representative of three independent experiments.

tethering IGF-1 to the SA-coated biosensor surface by Lys 27 or Gly 1 constrained the ligand molecule such that access by IGFBP-2 and IGFBP-3 was hindered. On this basis, both Gly 1 and Lys 27 must be accessible for binding to occur, as is the case when $N^{\epsilon Lys65/68b}$-IGF-1 is coated on the SA-coated surface. On the basis of the locations of the Gly 1 and Lys 27 residues, these results support a role for the IGFBP-binding domain and IGF-1R-binding domain, in IGF-1 binding to IGFBP-2 and IGFBP-3.

*Comparison of biotinylated IGF-1 and $^{125}$I-IGF-1 in Ligand Blot Analysis.* Because $N^{\epsilon Lys65/68b}$-IGF-1 demonstrated a robust signal in ligand blot studies, we next determined whether it had an equivalent activity compared to $^{125}$I-IGF-1. As shown in Figure 11, $N^{\epsilon Lys65/68b}$-IGF-1 (lower panel) demonstrated comparable signal intensity to $^{125}$I-IGF-1 (upper panel) in detecting increasing doses of IGFBP-2 and IGFBP-3. Significantly, the biotin-based ligand blot was developed for 1−30 min following addition of ECL reagent, while the $^{125}$I-IGF-1-based ligand blot required a 2-week exposure to X-ray film. Furthermore, biotinylated IGF-1 derivatives are stable at −20 C. These results validate the use of $N^{\epsilon Lys65/68b}$-IGF-1 as a more effective substitute for $^{125}$I-IGF-1 in ligand blot analyses.

## DISCUSSION

In this paper, we have shown that selectively biotinylated IGF-1 is both a novel tool for analysis of the IGFBPs in general as well as for the elucidation of specific IGF-1/IGFBP contact sites. IGF-1 residues Gly 1, Lys 27, Lys 65, and Lys 68 were selectively biotinylated. Gly 1 is within the N-terminal tripeptide (Gly-Pro-Glu) of IGF-1, flanking the Glu 3 residue, which is essential for high-affinity binding to the IGFBPs (*26*). Lys 27 flanks the IGF-1R-binding domain, supported by Yip et al., who showed the specific photoincorporation of $N^{\epsilon Lys27}$-monoazidobenzoyl-IGF-1 into

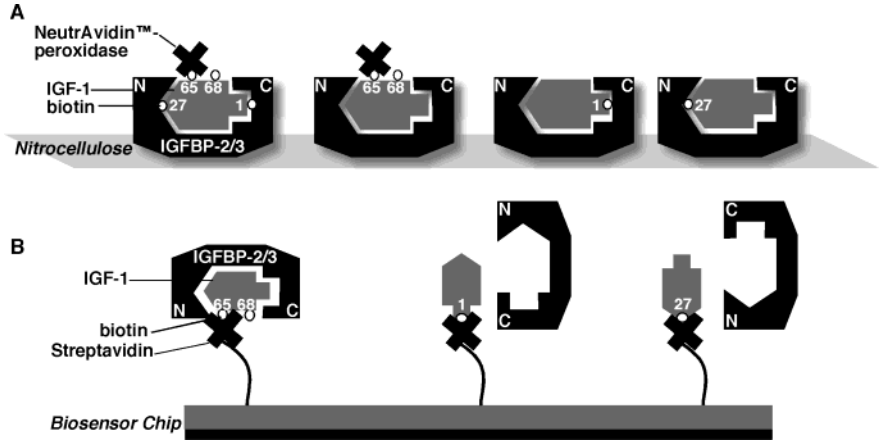


FIGURE 12: Schematic depiction of ligand blot and BIAcore results. (A) Diagram depicts binding of NeutrAvidin-peroxidase to IGF-1 via biotin on Lys 65 and Lys 68 but not Gly 1 or Lys 27, following IGF-1/IGFBP complex formation in the ligand blot. (B) For BIAcore analysis, individual species of monobiotinylated IGF-1 were immobilized in individual flowcells of a SA-coated biosensor chip, as shown. IGF-1 tethered by biotin at the Gly 1 or Lys 27 position did not appreciably bind IGFBP-2 or IGFBP-3, while IGF-1 tethered by biotin at Lys 65 or Lys 68 was able to significantly bind these IGFBPs. For simplicity, NeutrAvidin-peroxidase/SA is pictured bound to IGF-1 via Lys 65. Because $N^{\epsilon Lys68b}$-IGF-1 was also present during immobilization to the biosensor chip and in ligand blotting, a portion of the NeutrAvidin-peroxidase/SA was bound to IGF-1 by the biotin on Lys 68. As illustrated, Gly 1, within the IGFBP-binding domain, and Lys 27, near the IGF-1R-binding domain, participate in binding to IGFBP-2 and IGFBP-3.

the IGF-1R α subunit in Rat-1 fibroblast plasma membranes (*50*). Lys 65 and Lys 68 are positioned within the D region (*52*), outside both the IGFBP-binding domain and the IGF-1R-binding domain. Our data indicated the involvement of both the IGFBP-binding domain and the IGF-1R-binding domain on IGF-1 (Figure 1) in the interaction of IGF-1 with IGFBP-2 and IGFBP-3.

Solid-phase-binding analysis demonstrated that all three monobiotinylated derivatives displayed high affinity for IGFBP-2 and IGFBP-3, comparable to native IGF-1. In contrast, $N^{\alpha Gly1b}$-IGF-1 and $N^{\epsilon Lys27b}$-IGF-1 exhibited decreased labeling of IGFBP-2 and IGFBP-3 compared with $N^{\epsilon Lys65/68b}$-IGF-1 and QB-IGF-1 in ligand blot analysis. It was determined through the synthesis and examination of LC-biotin versions of these derivatives that the decreased labeling obtained with $N^{\alpha Gly1b}$-IGF-1 and $N^{\epsilon Lys27b}$-IGF-1 was not due to decreased binding affinity. Rather, the decreased labeling reflected NeutrAvidin-peroxidase inaccessibility to the biotin. This, in turn, suggested that Gly 1, Lys 27, and/or the domains within their vicinities contact IGFBP-2 and IGFBP-3 (Figure 12A). Conversely, $N^{\epsilon Lys65/68b}$-IGF-1 and $N^{\epsilon Lys65/68}$(LC-biotin)-IGF-1 demonstrated equivalent labeling of IGFBP-2 and IGFBP-3, suggesting that the region containing Lys 65 and Lys 68 is not a direct participant in IGFBP-2 and IGFBP-3 binding. This is consistent with NMR (*24*, *53*) and X-ray crystal (*34*) structures for IGF-1; in each case, the D region containing Lys 65 and Lys 68 is in contact with the solvent. BIAcore analysis allowed us to examine the binding interaction between IGF-1 and the IGFBPs in a manner distinct from ligand blotting. Instead of immobilizing the IGFBP in multiple orientations onto nitrocellulose, we tethered the ligand in a defined and uniform configuration; i.e., all immobilized ligand was attached by a single biotinylated amino acid. IGFBP-2 and IGFBP-3 established high-affinity, stable interactions with SA-immobilized $N^{\epsilon Lys65/68b}$-IGF-1, while IGFBP-2 and IGFBP-3 binding was either not observed (IGFBP-2) or was minimal and unstable (IGFBP-3) to SA-immobilized $N^{\alpha Gly1b}$-IGF-1 or $N^{\epsilon Lys27b}$-IGF-1. These data suggested that the orientation of $N^{\alpha Gly1b}$-IGF-1 or $N^{\epsilon Lys27b}$-IGF-1, when immobilized on the SA sensor chip, was unsuitable for high-affinity IGFBP-2 and IGFBP-3 binding, presumably because of the steric hindrance/constraint of IGF-1 by SA (Figure 12B). Ligand blot and BIAcore analyses together underscore that Gly 1, Lys 27, and/or their respective binding domains contact IGFBP-2 and IGFBP-3, while Lys 65 and Lys 68 do not. Our data corroborate evidence that Gly 1 is located in a region required for IGFBP binding (*26*). However, the involvement of IGF-1R binding domain residues of IGF-1 in IGFBP binding has not been previously described. Furthermore, our ligand blot and BIAcore data suggest that IGFBP-2 and IGFBP-3 have similar but somewhat unique structural requirements for binding IGF-1, which is in agreement with observations in the literature, as discussed below.

The homologous N termini of IGFBP-3 and IGFBP-5 have been shown to possess IGF-binding activity. Competition binding studies showed an ~20−40-fold reduction in IGF-1- and IGF-2-binding affinity when either the C terminus, mid-region, or both were deleted from IGFBP-3 compared to the intact protein (*33*). Therefore, the N-terminal fragment retained some affinity for IGF-1 and IGF-2. Imai et al. (*36*) demonstrated a reduction in the inhibition of IGF-1-dependent cell migration, DNA synthesis, and IGF-1R phosphorylation with amino acid substitutions of IGFBP-5 residues 68−74 and the homologous residues in IGFBP-3. BIAcore analysis of N-terminal, C-terminal, and mid-region fragments of IGFBP-5 corroborated this by showing that only the N-terminal fragments retain IGF-1 and IGF-2 binding; this binding was reduced 10−200-fold compared with intact IGFBP-5 (*35*). NMR analysis of an N-terminal fragment of IGFBP-5 (residues 40−92) in the absence or presence of IGF-2 suggested that the IGF-binding site may involve Val 49, Tyr 50, Pro 62, and Lys 68 to Leu 75 in IGFBP-5 (*34*, *35*). Most recently, the crystal structure of the complex of IGF-1 bound to the N-terminal domain of IGFBP-5 has been reported (*34*).

The C terminus of IGFBP-2 has been implicated in IGF binding. IGFBP-2 mutants truncated by 14, 36, or 48 residues

from the C terminus were shown to bind IGF-1 with the same affinity as intact IGFBP-2 in ligand blot and competition binding analyses. However, a mutant missing 63 residues from its C-terminal end exhibited a profound loss of binding affinity for IGF-1 (*38*). IGF-1 photoprobes derivatized at the Gly 1 position were incorporated at positions 266−287 and 212−227 of IGFBP-2, implicating the C terminus as a point of contact of IGFBP-2 with Gly 1 of IGF-1 (*30*). Ho and Baxter (*39*) isolated two C-terminal fragments of IGFBP-2 (14−15 kDa) from human milk, which have partial affinity (10-fold lower) for IGF-1 and IGF-2 in ligand blot and solution binding studies. IGF-2 residues 1−6 were absolutely required for this interaction, suggesting that the N-terminal residues of IGF interact directly with the C terminus of IGFBP-2. In summary, evidence indicates that both the N- and C-terminal domains of the IGFBPs are involved in IGF-1 binding and that IGFBP-2 and IGFBP-3 may have unique requirements for binding IGF-1. The differential labeling of IGFBP-2 and IGFBP-3 by the three monobiotinylated derivatives in ligand blotting in conjunction with the simliar $EC_{50}$ values that they exhibited in solid-phase-binding assays specifically suggest the novel concept that IGFBP-2 and IGFBP-3 interact with both the IGFBP-binding domain and the IGF-1R-binding domain on IGF-1.

Support for the participation of both binding domains on IGF-1 in interacting with IGFBP-2 and IGFBP-3 comes from several studies that have directly reported the involvement of both the N and C termini of the IGFBPs in IGF binding. Deletion of residues 1−60 of IGFBP-1 resulted in a loss of IGF-1-binding activity. Introduction of a point mutation at Cys 38 had a similar effect (*37*, *54*). Removal of the distal 20 residues from the C-terminal end of IGFBP-1 similarly resulted in the loss of IGF-1-binding activity based on ligand blot (*37*). Point mutation of Cys 226 abolished IGF binding, indicating the importance of disulfide bonding on IGFBP structure and function (*37*). Shand et al. (*42*) reported that the addition of Gly 203 and Gln 209 mutations to the N-terminal IGFBP-5 mutant described by Kalus et al. (*35*) resulted in a cumulative decrease in IGF binding. Most recently, co-incubation of N- and C-terminal fragments of IGFBP-3 was found to reconstitute IGF-binding affinity that was not significantly different from that of intact IGFBP-3 (*41*). Carrick et al. (*40*), through BIAcore analysis of bovine IGFBP-2 fragments, suggested that both the N and C termini contact the known binding-protein-binding domain of IGF-1.

Although mutagenesis data do not suggest the involvement of the IGF-1R-binding domain on IGF-1 in IGFBP binding, evidence for this possibility is based on the homology of the IGF-1R-binding domain on IGF-1 to the IR-binding domain on insulin. It has been reported that IGFBP-7/mac25 has a 100-fold greater affinity for insulin than do IGFBPs 1−6. Yamanaka et al. have shown that IGFBP-7/mac25 and an N-terminal fragment of IGFBP-3 (1−87) but not intact IGFBP-3 are able to inhibit insulin-dependent phosphorylation of the IR and IRS-1 (*17*). They also reported that both $^{125}$I-insulin or $^{125}$I-IGFs could be displaced from IGFBP-3 or IGFBP-7/mac25 by insulin or the IGFs, suggesting that these proteins bind at a site common to both the IGFs and insulin. When taken together, this suggests that the N terminus of IGFBP-3 may interact with the IR-binding domain on insulin and likewise the homologous domain on IGF-1. However, other reports demonstrate the possible interaction of the N terminus of IGFBP-3 and IGFBP-5 with the IGFBP-binding domain on IGF-2 (*34*). It should be noted that IGFBP-5 (40−92) was reported to inhibit IGF-1-stimulated IGF-1R phosphorylation, suggesting that this fragment is either binding to the IGF-1R-binding domain or that its interaction with the IGFBP-binding domain results in a loss of IGF-1R-binding activity. Clearly, additional work needs to be done to resolve this issue, including three-dimensional structural analysis of IGF-1 binding to intact IGFBP-2 and IGFBP-3.

In summary, this study presents a method for the purification of $N^{\epsilon Lys65/68b}$-IGF-1, a novel reagent with applicability to the study of IGFBPs, having several advantages over $^{125}$I-IGF-1. $^{125}$I-IGF-1 has been the ligand of choice in ligand blot protocols for many years (*48*). More recently, biotinylated IGF-1 has surfaced as an alternative to iodinated IGF-1 (*55*−*57*). Our study validates the need for purification of the biotinylated species and demonstrates that $N^{\epsilon Lys65/68b}$-IGF-1 is the optimal ligand for detection of IGFBPs by ligand blotting. We also describe the use of selectively biotinylated derivatives of IGF-1 to examine IGF-1/IGFBP interactions. Such site-specific modification has been reported by other investigators to study specific protein interactions (*58*, *59*) and protein topology (*60*). This report builds on the representation of IGF and insulin binding to the IGFBPs by Yamanaka et al. (*17*) as well as on our previously described model for IGFBP-2 binding to IGF-1 (*30*) and extends it to IGFBP-3 (Figure 12). We have demonstrated the involvement of the IGFBP-binding domain and IGF-1R-binding domain in IGF-1 binding to IGFBP-2 and IGFBP-3. We plan to determine the specific domains on IGFBP-2 and IGFBP-3 that interact with the IGFBP-binding domain and the IGF-1R-binding domain on IGF-1 using N- and C-terminal fragments of these IGFBPs in ligand-binding studies with selectively biotinylated IGF-1. We will then extend these studies to insulin and IGF-2. These analyses will provide important information to aid in the design of IGFBP-based therapeutics.

## ACKNOWLEDGMENT

We thank Genentech Inc. for generously providing recombinant human IGF-1. We also thank Kevin L. Schey, Ph.D. and the members of the MUSC Mass Spectrometry Facility for assistance with MALDI−TOF MS and MALDI−TOF−TOF MS analysis of IGF-1 fragments. We express gratitude to Christian Knaak, Ph.D. of the MUSC Biomolecular Resource Facility, (W. Scott Argraves, Ph.D., Director) for assistance with BIAcore experimentation and interpretation. We also thank the members of the Rosenzweig laboratory for many thoughtful discussions.

## REFERENCES

1. Humbel, R. E. (1990) Insulin-like growth factors I and II, *Eur. J. Biochem. 190*, 445−462.
2. Baker, J., Liu, J., Robertson, E. J., and Efstratiadis, A. (1993) Role of the insulin-like growth factors in embryonic and postnatal growth, *Cell 75*, 73−82.
3. Daughaday, W. H., and Rotwein, P. (1989) Insulin-like growth factors I and II. Peptide, messanger ribonucleic acid and gene structures, serum, and tissue concentrations, *Endocr. Rev. 10*, 68−91.

4. D′Ercole, A. J. (1996) Insulin-like growth factors and their receptors in growth, *Endocrinol. Metab. Clin. North Am. 25*, 573−590.
5. Jones, J. I., and Clemmons, D. R. (1995) Insulin-like growth factors and their binding proteins: Biological actions, *Endocr. Rev. 16*, 3−34.
6. Imai, Y., Busby, W. H., Jr., Smith, C. E., Clarke, J. B., Garmong, A. J., Horwitz, G. D., Rees, C., and Clemmons, D. R. (1997) Protease-resistant form of insulin-like growth factor-binding protein 5 is an inhibitor of insulin-like growth factor-I actions on porcine smooth muscle cells in culture, *J. Clin. Invest. 100*, 2596−2605.
7. Kodama, Y., Baxter, R. C., and Martin, J. L. (2002) Insulin-like growth factor-I inhibits cell growth in the a549 non-small lung cancer cell line, *Am. J. Respir. Cell Mol. Biol. 27*, 336−344.
8. Figueroa, J. A., Sharma, J., Jackson, J. G., McDermott, M. J., Hilsenbeck, S. G., and Yee, D. (1993) Recombinant insulin-like growth factor binding protein-1 inhibits IGF-I, serum, and estrogen-dependent growth of MCF-7 human breast cancer cells, *J. Cell. Physiol. 157*, 229−236.
9. Van den Berg, C. L., Cox, G. N., Stroh, C. A., Hilsenbeck, S. G., Weng, C. N., McDermott, M. J., Pratt, D., Osborne, C. K., Coronado-Heinsohn, E. B., and Yee, D. (1997) Polyethylene glycol conjugated insulin-like growth factor binding protein-1 (IGFBP-1) inhibits growth of breast cancer in athymic mice, *Eur. J. Cancer 33*, 1108−1113.
10. Arteaga, C. L., Kitten, L. J., Coronado, E. B., Jacobs, S., Kull, F. C., Jr., Allred, D. C., and Osborne, C. K. (1989) Blockade of the type I somatomedin receptor inhibits growth of human breast cancer cells in athymic mice, *J. Clin. Invest. 84*, 1418−1423.
11. Sachdev, D., Li, S. L., Hartell, J. S., Fujita-Yamaguchi, Y., Miller, J. S., and Yee, D. (2003) A chimeric humanized single-chain antibody against the type I insulin-like growth factor (IGF) receptor renders breast cancer cells refractory to the mitogenic effects of IGF-I, *Cancer Res. 63*, 627−635.
12. Guler, H. P., Zapf, J., Schmid, C., and Froesch, E. R. (1989) Insulin-like growth factors I and II in healthy man. Estimations of half-lives and production rates, *Acta Endocrinol. 121*, 753−758.
13. Hong, J., Zhang, G., Dong, F., and Rechler, M. M. (2002) Insulin-like growth factor (IGF)-binding protein-3 mutants that do not bind IGF-I or IGF-II stimulate apoptosis in human prostate cancer cells, *J. Biol. Chem. 277*, 10489−10497.
14. Rajah, R., Valentinis, B., and Cohen, P. (1997) Insulin-like growth factor (IGF)-binding protein-3 induces apoptosis and mediates the effects of transforming growth factor-$\beta$1 on programmed cell death through a p53- and IGF-independent mechanism, *J. Biol. Chem. 272*, 12181−12188.
15. Cohen, P., Graves, H. C., Peehl, D. M., Kamarei, M., Giudice, L. C., and Rosenfeld, R. G. (1992) Prostate-specific antigen (PSA) is an insulin-like growth factor binding protein-3 protease found in seminal plasma, *J. Clin. Endocrinol. Metab. 75*, 1046−1053.
16. Collett-Solberg, P. F., and Cohen, P. (1996) The role of the insulin-like growth factor binding proteins and the IGFBP proteases in modulating IGF action, *Endocrinol. Metab. Clin. North Am. 25*, 591−614.
17. Yamanaka, Y., Wilson, E. M., Rosenfeld, R. G., and Oh, Y. (1997) Inhibition of insulin receptor activation by insulin-like growth factor binding proteins, *J. Biol. Chem. 272*, 30729−30734.
18. Hwa, V., Oh, Y., and Rosenfeld, R. G. (1999) The insulin-like growth factor-binding protein (IGFBP) superfamily, *Endocr. Rev. 20*, 761−787.
19. Smith, G. L., Doherty, A. P., Mitchell, H., Hanham, I. W., Christmas, T. J., and Epstein, R. J. (1999) Inverse relation between prostate-specific antigen and insulin-like growth factor-binding protein 3 in bone metastases and serum of patients with prostate cancer, *Lancet 354*, 2053−2054.
20. Ouban, A., Muraca, P., Yeatman, T., and Coppola, D. (2003) Expression and distribution of insulin-like growth factor-1 receptor in human carcinomas, *Hum. Pathol. 34*, 803−808.
21. Chan, J. M., Stampfer, M. J., Giovannucci, E., Gann, P. H., Ma, J., Wilkinson, P., Hennekens, C. H., and Pollak, M. (1998) Plasma insulin-like growth factor-I and prostate cancer risk: A prospective study, *Science 279*, 563−566.
22. Hankinson, S. E., Willett, W. C., Colditz, G. A., Hunter, D. J., Michaud, D. S., Deroo, B., Rosner, B., Speizer, F. E., and Pollak, M. (1998) Circulating concentrations of insulin-like growth factor-I and risk of breast cancer, *Lancet 351*, 1393−1396.
23. Mauro, L., Salerno, M., Morelli, C., Boterberg, T., Bracke, M. E., and Surmacz, E. (2003) Role of the IGF-I receptor in the regulation of cell−cell adhesion: Implications in cancer development and progression, *J. Cell. Physiol. 194*, 108−116.
24. Cooke, R. M., Harvey, T. S., and Campbell, I. D. (1991) Solution structure of human insulin-like growth factor 1: A nuclear magnetic resonance and restrained molecular dynamics study, *Biochemistry 30*, 5484−5491.
25. Blundell, T. L., Bedarkar, S., Rinderknecht, E., and Humbel, R. E. (1978) Insulin-like growth factor: A model for tertiary structure accounting for immunoreactivity and receptor binding, *Proc. Natl. Acad. Sci. U.S.A. 75*, 180−184.
26. Szabo, L., Mottershead, D. G., Ballard, F. J., and Wallace, J. C. (1988) The bovine insulin-like growth factor (IGF) binding protein purified from conditioned medium requires the N-terminal tripeptide in IGF-1 for binding, *Biochem. Biophys. Res. Commun. 151*, 207−214.
27. Bayne, M. L., Applebaum, J., Chicchi, G. G., Hayes, N. S., Green, B. G., and Cascieri, M. A. (1988) Structural analogs of human insulin-like growth factor I with reduced affinity for serum binding proteins and the type 2 insulin-like growth factor receptor, *J. Biol. Chem. 263*, 6233−6239.
28. Cascieri, M. A., Chicchi, G. G., Applebaum, J., Green, B. G., Hayes, N. S., and Bayne, M. L. (1989) Structural analogs of human insulin-like growth factor (IGF) I with altered affinity for type 2 IGF receptors, *J. Biol. Chem. 264*, 2199−2202.
29. Bagley, C. J., May, B. L., Szabo, L., McNamara, P. J., Ross, M., Francis, G. L., Ballard, F. J., and Wallace, J. C. (1989) A key functional role for the insulin-like growth factor 1 N-terminal pentapeptide, *Biochem. J. 259*, 665−671.
30. Horney, M. J., Evangelista, C. A., and Rosenzweig, S. A. (2001) Synthesis and characterization of insulin-like growth factor (IGF)-1 photoprobes selective for the IGF-binding proteins (IGFBPS). Photoaffinity labeling of the IGF-binding domain on IGFBP-2, *J. Biol. Chem. 276*, 2880−2889.
31. Cascieri, M. A., Chicchi, G. G., Applebaum, J., Hayes, N. S., Green, B. G., and Bayne, M. L. (1988) Mutants of human insulin-like growth factor I with reduced affinity for the type 1 insulin-like growth factor receptor, *Biochemistry 27*, 3229−3233.
32. Maly, P., and Luthi, C. (1988) The binding sites of insulin-like growth factor I (IGF-I) to type I IGF receptor and to a monoclonal antibody. Mapping by chemical modification of tyrosine residues, *J. Biol. Chem. 263*, 7068−7072.
33. Firth, S. M., Ganeshprasad, U., and Baxter, R. C. (1998) Structural determinants of ligand and cell surface binding of insulin-like growth factor-binding protein-3, *J. Biol. Chem. 273*, 2631−2638.
34. Zeslawski, W., Beisel, H. G., Kamionka, M., Kalus, W., Engh, R. A., Huber, R., Lang, K., and Holak, T. A. (2001) The interaction of insulin-like growth factor-I with the N-terminal domain of IGFBP-5, *EMBO J. 20*, 3638−3644.
35. Kalus, W., Zweckstetter, M., Renner, C., Sanchez, Y., Georgescu, J., Grol, M., Demuth, D., Schumacher, R., Dony, C., Lang, K., and Holak, T. A. (1998) Structure of the IGF-binding domain of the insulin-like growth factor-binding protein-5 (IGFBP-5): Implications for IGF and IGF-I receptor interactions, *EMBO J. 17*, 6558−6572.
36. Imai, Y., Moralez, A., Andag, U., Clarke, J. B., Busby, W. H., Jr., and Clemmons, D. R. (2000) Substitutions for hydrophobic amino acids in the N-terminal domains of IGFBP-3 and -5 markedly reduce IGF-I binding and alter their biologic actions, *J. Biol. Chem. 275*, 18188−18194.
37. Brinkman, A., Kortleve, D. J., Zwarthoff, E. C., and Drop, S. L. (1991) Mutations in the C-terminal part of insulin-like growth factor (IGF)-binding protein-1 result in dimer formation and loss of IGF binding capacity, *Mol. Endocrinol. 5*, 987−994.
38. Forbes, B. E., Turner, D., Hodge, S. J., McNeil, K. A., Forsberg, G., and Wallace, J. C. (1998) Localization of an insulin-like growth factor (IGF) binding site of bovine IGF binding protein-2 using disulfide mapping and deletion mutation analysis of the C-terminal domain, *J. Biol. Chem. 273*, 4647−4652.
39. Ho, P. J., and Baxter, R. C. (1997) Characterization of truncated insulin-like growth factor-binding protein-2 in human milk, *Endocrinology 138*, 3811−3818.
40. Carrick, F. E., Forbes, B. E., and Wallace, J. C. (2001) BIAcore analysis of bovine insulin-like growth factor (IGF)-binding protein-2 identifies major IGF binding site determinants in both the amino- and carboxyl-terminal domains, *J. Biol. Chem. 276*, 27120−27128.

41. Payet, L. D., Wang, X. H., Baxter, R. C., and Firth, S. M. (2003) Amino- and carboxyl-terminal fragments of insulin-like growth factor (IGF) binding protein-3 cooperate to bind IGFs with high affinity and inhibit IGF receptor interactions, *Endocrinology 144*, 2797−2806.
42. Shand, J. H., Beattie, J., Song, H., Phillips, K., Kelly, S. M., Flint, D. J., and Allan, G. J. (2003) Specific amino acid substitutions determine the differential contribution of the N- and C-terminal domains of insulin-like growth factor (IGF)-binding protein-5 in binding IGF-I, *J. Biol. Chem. 278*, 17859−17866.
43. Urlaub, G., Kas, E., Carothers, A. M., and Chasin, L. A. (1983) Deletion of the diploid dihydrofolate reductase locus from cultured mammalian cells, *Cell 33*, 405−412.
44. Han, J. C., and Han, G. Y. (1994) A procedure for quantitative determination of tris(2-carboxyethyl)phosphine, an odorless reducing agent more stable and effective than dithiothreitol, *Anal. Biochem. 220*, 5−10.
45. Honegger, A., and Humbel, R. E. (1986) Insulin-like growth factors I and II in fetal and adult bovine serum. Purification, primary structures, and immunological cross-reactivities, *J. Biol. Chem. 261*, 569−575.
46. Forsberg, G., Palm, G., Ekebacke, A., Josephson, S., and Hartmanis, M. (1990) Separation and characterization of modified variants of recombinant human insulin-like growth factor I derived from a fusion protein secreted from *Escherichia coli*, *Biochem. J. 271*, 357−363.
47. Laemmli, U. K. (1970) Cleavage of structural proteins during the assembly of the head of bacteriophage T4, *Nature 227*, 680−685.
48. Hossenlopp, P., Seurin, D., Segovia-Quinson, B., Hardouin, S., and Binoux, M. (1986) Analysis of serum insulin-like growth factor binding proteins using western blotting: Use of the method for titration of the binding proteins and competitive binding studies, *Anal. Biochem. 154*, 138−143.
49. Horney, M. J., Shirley, D. W., Kurtz, D. T., and Rosenzweig, S. A. (1998) Elevated glucose increases mesangial cell sensitivity to insulin-like growth factor I, *Am. J. Physiol. 274*, F1045−F1053.
50. Yip, C. C., Hsu, H., Olefsky, J. M., and Seely, L. (1993) Preparation of N epsilon B28-monoazidobenzoyl insulin-like growth factor I and photoaffinity labeling of insulin-like growth factor I receptor, *Peptides 14*, 325−330.
51. Slomiany, M. G., and Rosenzweig, S. A. (2004) Induced VEGF and IGFBP-3 sretion correlates with increased HIF-1-a nuclear translocation in the retinal pigment epithelial cell line D407, *Ophthalmol. Vis. Sci.* in press.
52. Brzozowski, A. M., Dodson, E. J., Dodson, G. G., Murshudov, G. N., Verma, C., Turkenburg, J. P., de Bree, F. M., and Dauter, Z. (2002) Structural origins of the functional divergence of human insulin-like growth factor-I and insulin, *Biochemistry 41*, 9389−9397.
53. Schaffer, M. L., Deshayes, K., Nakamura, G., Sidhu, S., and Skelton, N. J. (2003) Complex with a phage display-derived peptide provides insight into the function of insulin-like growth factor I, *Biochemistry 42*, 9324−9334.
54. Brinkman, A., Kortleve, D. J., Schuller, A. G., Zwarthoff, E. C., and Drop, S. L. (1991) Site-directed mutagenesis of the N-terminal region of IGF binding protein 1; analysis of IGF binding capability, *FEBS Lett. 291*, 264−268.
55. Grulich-Henn, J., Spiess, S., Heinrich, U., Schonberg, D., and Bettendorf, M. (1998) Ligand blot analysis of insulin-like growth factor-binding proteins using biotinylated insulin-like growth factor-I, *Horm. Res. 49*, 1−7.
56. Fowlkes, J. L., and Serra, D. (1996) A rapid, non-radioactive method for the detection of insulin-like growth factor binding proteins by Western ligand blotting, *Endocrinology 137*, 5751−5754.
57. Op De Beeck, L., Verlooy, J. E., Van Buul-Offers, S. C., and Du Caju, M. V. (1997) Detection of serum insulin-like growth factor binding proteins on western ligand blots by biotinylated IGF and enhanced chemiluminescence, *J. Endocrinol. 154*, R1−R5.
58. Pepinsky, R. B., Rayhorn, P., Day, E. S., Dergay, A., Williams, K. P., Galdes, A., Taylor, F. R., Boriack-Sjodin, P. A., and Garber, E. A. (2000) Mapping sonic hedgehog-receptor interactions by steric interference, *J. Biol. Chem. 275*, 10995−11001.
59. Toedt, G. H., Krishnan, R., and Friedhoff, P. (2003) Site-specific protein modification to identify the MutL interface of MutH, *Nucleic Acids Res. 31*, 819−825.
60. Song, J., Midson, C., Blachly-Dyson, E., Forte, M., and Colombini, M. (1998) The topology of VDAC as probed by biotin modification, *J. Biol. Chem. 273*, 24406−24413.

BI049082K